
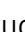






# CIP2A deficiency promotes depression-like behaviors in mice through inhibition of dendritic arborization

Wen-Ting Hu<sup>1,2,†</sup>, Zhen-Yu Liuyang<sup>1,3,†</sup>, Yuan Tian<sup>4</sup> , Jia-Wei Liang<sup>1</sup>, Xiao-Lin Zhang<sup>1</sup>, Hui-Liang Zhang<sup>1</sup>, Guan Wang<sup>4</sup> , Yuda Huo<sup>4</sup>, Yang-Ping Shentu<sup>5</sup>, Jian-Zhi Wang<sup>1</sup>, Xiao-Chuan Wang<sup>1</sup> , You-ming Lu<sup>1,6</sup>, Jukka Westermarck<sup>7,8,9</sup> , Heng-Ye Man<sup>4,\*</sup>  & Rong Liu<sup>1,6,10,\*\*</sup> 

## Abstract

Major depressive disorder (MDD) is a severe mental illness. Decreased brain plasticity and dendritic fields have been consistently found in MDD patients and animal models; however, the underlying molecular mechanisms remain to be clarified. Here, we demonstrate that the deletion of cancerous inhibitor of PP2A (CIP2A), an endogenous inhibitor of protein phosphatase 2A (PP2A), leads to depression-like behaviors in mice. Hippocampal RNA sequencing analysis of CIP2A knockout mice shows alterations in the PI3K-AKT pathway and central nervous system development. In primary neurons, CIP2A stimulates AKT activity and promotes dendritic development. Further analysis reveals that the effect of CIP2A in promoting dendritic development is dependent on PP2A-AKT signaling. *In vivo*, CIP2A deficiency-induced depression-like behaviors and impaired dendritic arborization are rescued by AKT activation. Decreased CIP2A expression and impaired dendrite branching are observed in a mouse model of chronic unpredictable mild stress (CUMS). Indicative of clinical relevance to humans, CIP2A expression is found decreased in transcriptomes from MDD patients. In conclusion, we discover a novel mechanism that CIP2A deficiency promotes depression through the regulation of PP2A-AKT signaling and dendritic arborization.

**Keywords** AKT; CIP2A; dendritic arborization; depression; PP2A

**Subject Categories** Molecular Biology of Disease; Neuroscience; Signal Transduction

**DOI** 10.15252/embr.202254911 | Received 22 February 2022 | Revised 25 August 2022 | Accepted 4 October 2022 | Published online 28 October 2022

**EMBO Reports (2022) 23: e54911**

## Introduction

Major depressive disorder (MDD) is a complex and highly prevalent mental illness, which severely limits psychosocial functioning and decreases life quality of the affected individuals (Nestler *et al*, 2002; Price & Drevets, 2010; Sjöberg *et al*, 2017). The lifetime risk of depression is 15–18%, indicating that almost one in five people experiencing one episode of depression at some point in their lifetime. The 12-month prevalence of MDD is approximately 6% worldwide (Malhi & Mann, 2018). Effective treatments for MDD are limited due to poor mechanistic understanding of the disease. At present, the treatment of depression mainly relies on the regulation of the monoamine system; however, about 30% of depression patients have partial or complete resistance to this treatment. Therefore, further investigation on the molecular mechanisms of MDD is urgently needed (Dowlati *et al*, 2010; Brent, 2016).

Brain plasticity is the brain's ability to change structure and function, in which the establishment, maintenance, and remodeling of dendrite branching complexity is a key event (Kolb &

1 Department of Pathophysiology, Key Laboratory of Ministry of Education for Neurological Disorders, School of Basic Medicine, Tongji Medical College, Huazhong University of Science and Technology, Wuhan, China  
 2 Department of Pathology, Peking University Shenzhen Hospital, Shenzhen, China  
 3 Department of General Surgery, Sir Run Run Shaw Hospital, School of Medicine, Zhejiang University, Hangzhou, China  
 4 Department of Biology, Boston University, Boston, USA  
 5 Department of Nephrology, The First Affiliated Hospital of Wenzhou Medical University, Wenzhou, China  
 6 The Institute of Brain Research, Collaborative Innovation Center for Brain Science, Huazhong University of Science and Technology, Wuhan, China  
 7 Turku Bioscience Centre, University of Turku, Turku, Finland  
 8 Åbo Akademi University, Turku, Finland  
 9 Institute of Biomedicine, University of Turku, Turku, Finland  
 10 Department of Pediatrics, Tongji Hospital, Tongji Medical College, Huazhong University of Science and Technology, Wuhan, China  
 \*Corresponding author. Tel: +86 27 83692625; E-mail: rong.liu@hust.edu.cn  
 \*\*Corresponding author. Tel: +1 617 358 4284; E-mail: hman@bu.edu  
 †These authors contributed equally to this work

Whishaw, 1998). Impaired brain plasticity is a characteristic pathology in MDD (Duman, 2013; Xu *et al.*, 2016; Sedmak *et al.*, 2018). Brain imaging and postmortem autopsy show a decreased hippocampal volume in major depression patients, accompanied by a reduction in dendritic arborization and spine density (Kempton *et al.*, 2011; Duman & Aghajanian, 2012). In chronic stress-induced depression animal models, dendritic atrophy and spine loss are also significant in the prefrontal cortex (PFC) and hippocampus (Kempton *et al.*, 2011; Duman & Aghajanian, 2012; Abe-Higuchi *et al.*, 2016; Liang *et al.*, 2019). In addition, the rapid antidepressant actions of ketamine are associated with fast induction of synaptogenesis and reversal of brain atrophy in rodents exposed to chronic stress (Li *et al.*, 2010, 2011). These findings strongly suggest that the defect in dendritic arborization and synaptogenesis plays an important role in depression. Elucidation of the mechanisms underlying the deficits in dendritic development may disclose new molecular targets in MDD treatment.

The serine/threonine kinase AKT, also known as protein kinase B, is an important regulator of dendritic arborization/development and synaptogenesis (Jaworski *et al.*, 2005; Peineau *et al.*, 2007; Read & Gorman, 2009; Vanderplow *et al.*, 2021). Decreased AKT activity in neurons is associated with increased susceptibility to social defeat stress and is reversed by antidepressant treatment in rodents and in human (Krishnan *et al.*, 2008). In mice, AKT inhibition caused a striking reduction in basal dendritic spine density in the mPFC and the loss of different types of spines, reducing synaptic structural and functional plasticity (Ehm *et al.*, 2010; Vanderplow *et al.*, 2021). These findings indicate that AKT deficiency contributes to altered brain plasticity in depression; however, the precise upstream regulators remain to be explored.

Cancerous inhibitor of PP2A (CIP2A) is an endogenous inhibitor of protein phosphatase 2A (PP2A). As an oncoprotein, CIP2A promotes tumor cell growth through inhibiting the dephosphorylation of PP2A substrates, which are involved in cancer development (Junttila *et al.*, 2007; Puustinen & Jäättelä, 2014). CIP2A is expressed in human brains, with a high-level expression, especially in the hippocampus, but the role of CIP2A in the brain is not well understood (Junttila *et al.*, 2007). Previous studies have shown that CIP2A promotes the self-renewal and proliferation of neural progenitor cells (NPCs) through interacting with the PP2A dephosphorylation substrate *c-Myc* (Kerosuo *et al.*, 2010). Further, CIP2A overexpression has been shown to promote Alzheimer's disease (AD) development in mouse models (Shentu *et al.*, 2018, 2019). However, the role of CIP2A in psychiatric disorders is currently unknown.

In this study, we show an important role of CIP2A in dendritic development through PP2A-AKT signaling pathway. CIP2A deficiency leads to depression-like behavioral phenotypes and impairments in dendritic arborization, which can be rescued by AKT activation *in vivo*. Collectively, these findings reveal a novel molecular mechanism in the pathogenesis of depression.

## Results

### CIP2A deficiency induces depression-like behaviors in mice

To evaluate the role of CIP2A in the brain, we conducted a series of behavioral tests on CIP2A knockout mice (6-month-old, CIP2A-KO)

and age-matched wild-type control mice (C57-WT; Ventelä *et al.*, 2012; Fig 1A). The results showed that compared with the C57 WT mice, CIP2A-KO mice were lighter in body weight (Fig 1B) and had faster running speed and comparable running time in the rotarod test (Fig 1C and D). In the grip test and footprint assay, there was no significant difference between the two groups (Fig 1E–G). These data suggest that CIP2A deficiency does not induce impairment in motor ability in mice.

Next, we performed sucrose preference test to assess anhedonia of the mice. The results showed that the CIP2A knockout mice had reduced sucrose intake compared with control mice, indicating that CIP2A depletion induced anhedonia (Fig 1H and I). In forced swimming test, CIP2A knockout mice showed decreased struggling time (s) and increased immobility time (s) compared with the C57-WT mice (Fig 1J–L). In addition, in open field test, CIP2A knockout mice had decreased time in center (s) and reduced exploration behaviors (horizontal activity and vertical activity) compared with WT mice (Fig 1M–P). These results indicate that CIP2A deficiency induces depression-like behaviors in mice.

We also explored the impact of CIP2A depletion on spatial learning and memory through T maze and Morris water maze test (MWM). CIP2A knockout mice showed comparable change times in T maze and crossing times in MWM (Fig 1Q–T), indicating that CIP2A deficiency does not cause deficits in cognitive function. Taken together, these behavioral tests indicate that CIP2A deficiency can be implicated in the pathogenesis of depression in mouse models.

### Transcriptomes of CIP2A knockout mice and MDD patients reveal abnormalities in PI3K-AKT signaling

To gain more insight into the potential molecular mechanism of CIP2A deficiency in promoting depression, we performed RNA sequencing (RNA-seq) in mouse hippocampal tissues to examine genome-wide gene expression changes. Numerous differentially expressed genes (DEGs) were identified in mice with CIP2A deletion compared with controls (Fig 2A). Gene ontology (GO) analysis of DEGs revealed that downregulated genes were mostly enriched in biological processes involved in transmembrane transport, central nervous system development, and cilium movement (Fig 2B). In Fig 2C, Benjamini correction was further performed to show the significance of DEGs-enriched GO terms. KEGG analysis of DEGs showed that most of the DEGs were mainly enriched in the metabolic pathways, neuroactive ligand-receptor interaction, cytokine-cytokine receptor interaction, and PI3K-AKT signaling pathway (Fig 2D). Previous studies have suggested that MDD is related to increased neuronal atrophy, mainly due to the reduction in synaptic plasticity and defects in dendritic branching (Tavosanis, 2012; Duman, 2013). Moreover, dendritic arborization is regulated by a variety of signaling pathways, such as AKT signaling pathway, MAPK signaling pathway, and Wnt signaling pathway (Yu & Malenka, 2003; Kumar *et al.*, 2005; Rosso *et al.*, 2005; Read & Gorman, 2009). Thus, we further analyzed the transcriptome of MDD patient brains using available Gene Expression Omnibus (GEO) dataset (GSE54572) (Chang *et al.*, 2014; Data ref: Sibille, 2014a) and found that the DEGs were also significantly enriched in PI3K-AKT signaling pathway (Fig 2E). Finally, we analyzed the CIP2A gene expression in three GEO datasets (GSE54572, GSE54565, and GSE54571), which contain

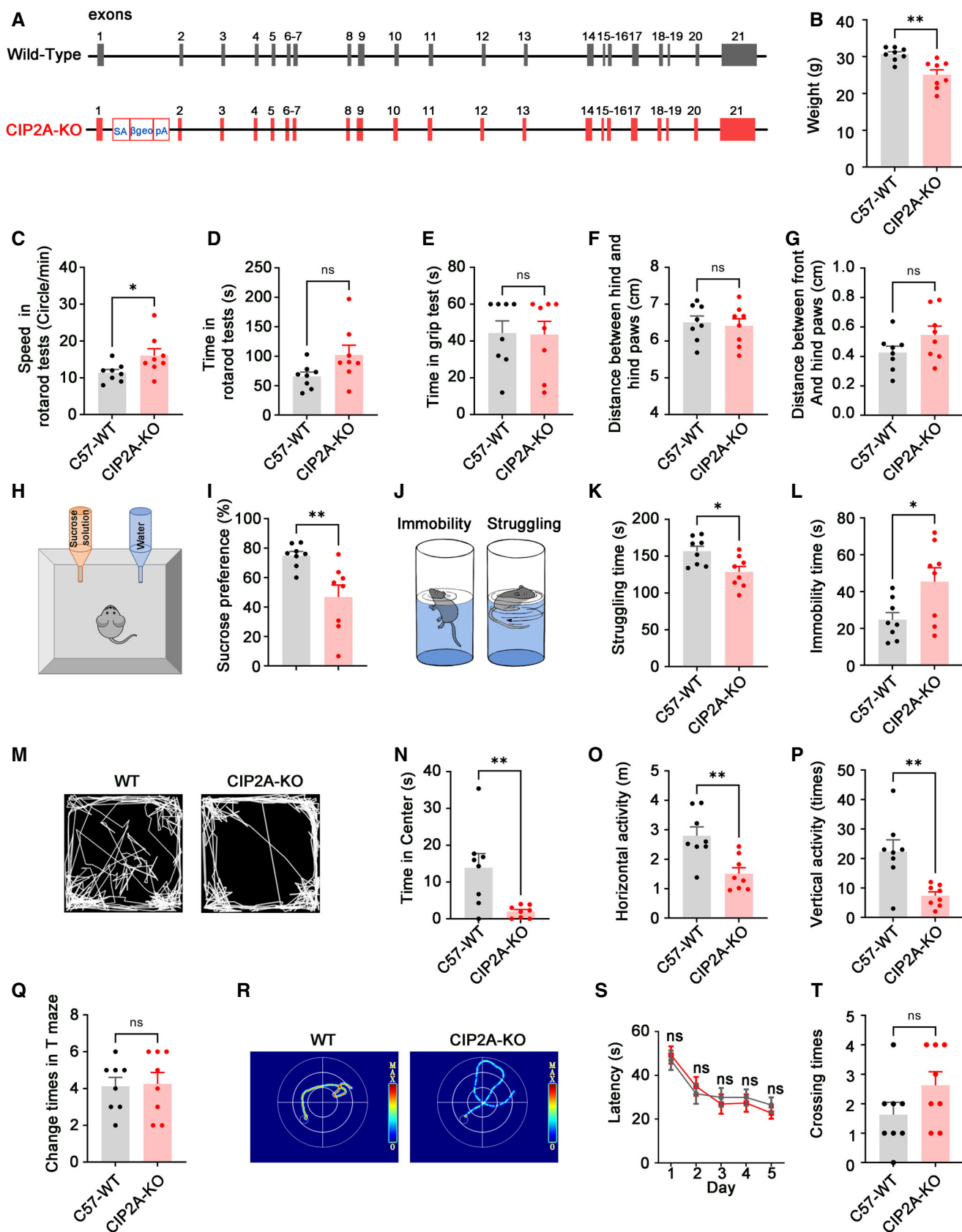


Figure 1.

**Figure 1. CIP2A deficiency induces depression-like behaviors in mice.**

- A Gene-trap strategy for CIP2A deletion in mice. The pGTOLxf gene-trap vector containing a splice acceptor site (SA),  $\beta$ -galactosidase reporter gene ( $\beta$ -geo), and a SV40 polyadenylation site (pA) was inserted in CIP2A locus intron 1 and resulted in disrupted CIP2A expression.
- B The body weight (g) of C57-WT mice and CIP2A-KO mice (male, 6-month-old).
- C, D The speed (circle/min) (C) and running time (s) (D) of the mice in rotarod test.
- E The mean time of the mice keep grabbing the pole in grip test.
- F, G The distance between hind and hind paws (cm) (F) and the distance between front and hind paws (cm) (G) in footprint assay.
- H, I The schematic diagram of sucrose preference test (H) and the sucrose preference ratio (%) of the mice in two groups (I).
- J–L The schematic diagram of forced swimming test (J), the struggling time (s) (K), and the immobility time (s) (L) in forced swimming test of the mice in two groups.
- M–P The representative searching trace (M), the time in center (s) (N), the horizontal activity (m) (O), and the vertical activity (times) (P) of the mice in open field test.
- Q The change times in T maze of the mice in two groups.
- R–T The mice were trained for 5 days with three trials per day and tested on day 7 in Morris water maze test (MWM). The representative searching trace on day 5 of the training trial (R), the latency of the mice to find the hidden platform (S), and the times of crossing the platform (T) in the testing trial.
- Data information: Data are presented as mean  $\pm$  SEM. ns, not significant; \* $P < 0.05$ , \*\* $P < 0.01$ ,  $n = 8$  mice/group,  $n$  represents biological replicates. For (B–G), (I), (K–L), (N–Q) and (T), data are analyzed by Student's *t*-test. For (S), data are analyzed by two-way repeated-measures ANOVA followed by Bonferroni's *post hoc* test.

the gene expression data of human brain anterior cingulate cortices from controls and MDD patients (Chang *et al*, 2014; Data ref: Sibille, 2014a; Data ref: Sibille, 2014b; Data ref: Sibille, 2014c). We found that compared with the control group, the expression of CIP2A in MDD patients had a tendency of reduction ( $P = 0.06$ , Fig 2F). Based on these data, we speculate that CIP2A deficiency may participate in MDD through dysregulation of PI3K-AKT signaling and dendritic arborization.

**CIP2A activates AKT in primary neurons and promotes dendritic development through PI3K-AKT pathway**

To verify our hypothesis, we explored the role of CIP2A in regulating AKT activity and dendritic development in neurons. First, the protein levels of CIP2A and active forms of AKT (AKT phosphorylated at Ser473) in different developmental stages were detected in cultured primary neurons. We found that the protein level of CIP2A was highly correlated with the AKT phosphorylation at Ser473. Furthermore, the peak expression of CIP2A and the AKT-S473 phosphorylation were on the DIV 5 of the cultured neurons, which was highly consistent with the time point of dendritic development (Fig 3A and B). Further immunofluorescence staining showed that CIP2A co-localized with MAP2 (a marker of dendrites) and AKT-S473, respectively, in primary hippocampal neurons (Fig 3C). Co-immunoprecipitation (Co-IP) result indicated the interaction of CIP2A with AKT and PP2A subunits (Fig 3D). To verify that CIP2A is able to activate AKT in neurons, we overexpressed CIP2A in cultured neurons through AAV infection. By Western blotting, we found that overexpression

of CIP2A increased the phosphorylation at AKT-S473 and activated AKT in primary neurons (Fig 3E).

Next, to investigate whether CIP2A could regulate the dendritic arborization and development directly, cultured hippocampal neurons were transfected with CIP2A plasmid on DIV 4 (Fig 3F). On DIV 7, the dendritic development was evaluated through analyzing the number, length, and complexity of the neurites. The results showed that the complexity of dendrite, the number of dendritic branches, the mean dendritic length, and the total dendritic length were all significantly increased in CIP2A-overexpressed neurons (Fig EV1A and B). The efficient overexpression of CIP2A by plasmid transfection, and activation of AKT by CIP2A, was also confirmed in N2a cells (Figs EV1C and D).

To further clarify that CIP2A regulates dendritic development through AKT activation, we used PI3K-specific inhibitor LY294002 (LY) to suppress the PI3K-AKT signaling. Primary hippocampal neurons were transfected with surface-EGFP or surface-EGFP and CIP2A plasmid at DIV 4, with or without LY294002 treatment for 3 days. Dendritic development of primary neurons was examined by fluorescence microscopy at DIV 7 (Fig 3G). We found that PI3K-AKT signaling inhibition significantly reduced the number, length, and complexity of the dendrites. However, the dendritic branching was not completely blocked, indicating that besides AKT, other factors are also involved in maintaining dendrite structure and promoting dendritic branching. But when AKT was inhibited, CIP2A was unable to enhance dendritic arborization/development any more (Fig 3H and I, LY versus LY + CIP2A), these results support that CIP2A shares a pathway with PI3K-AKT signaling in promoting dendritic development.

**Figure 2. Transcriptomes of CIP2A knockout mice and MDD patients reveal abnormalities in PI3K-AKT signaling.**

- A Volcano plot showing differentially expressed genes (DEGs) in hippocampus of CIP2A knockout mice and WT mice (red, upregulation; green, downregulation).
- B Gene Ontology analysis of downregulated genes by CIP2A deficiency showing the number of enriched genes. BP, biological process; CC, cellular component; MF, molecular function.
- C Gene Ontology analysis of downregulated genes by CIP2A deficiency with Benjamini correction showing the number and significance of enriched genes.
- D KEGG analysis of downregulated or upregulated genes by CIP2A deletion in mice,  $n = 3$  for (A–D),  $n$  represents biological replicates.
- E KEGG analysis of DEGs in human brain anterior cingulate cortices from controls and MDD patients. The gene expression data were obtained from GEO dataset GSE54572. Benjamini correction was performed to show the number and significance of enriched genes (Control  $n = 12$ , MDD patient  $n = 12$ ).
- F Transcriptional level of CIP2A in anterior cingulate cortices from controls and MDD patients in GSE54572, GSE54565, and GSE54571 dataset (Control  $n = 41$ ; MDD patient  $n = 41$ ); data are analyzed by Student's *t*-test.

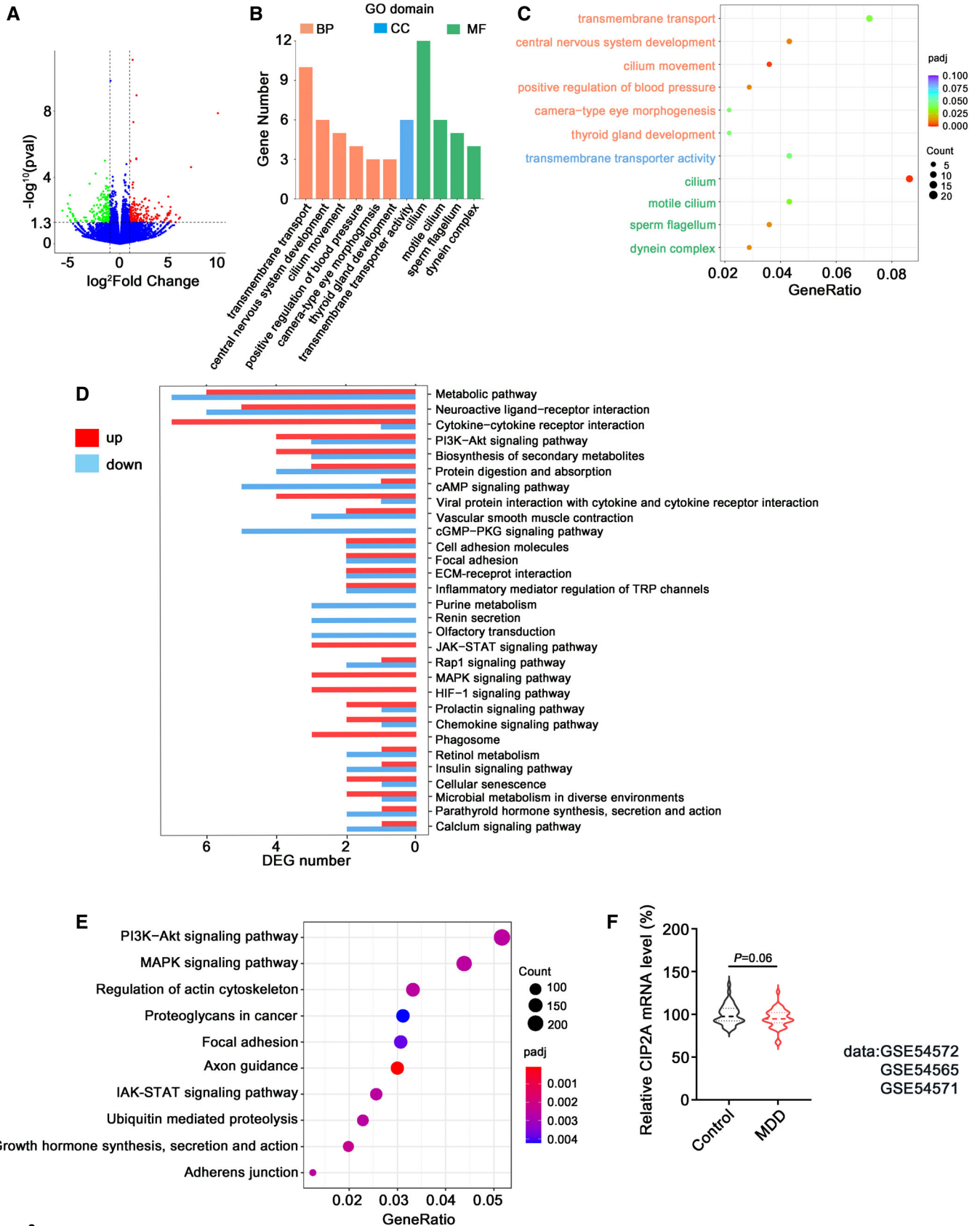


Figure 2.

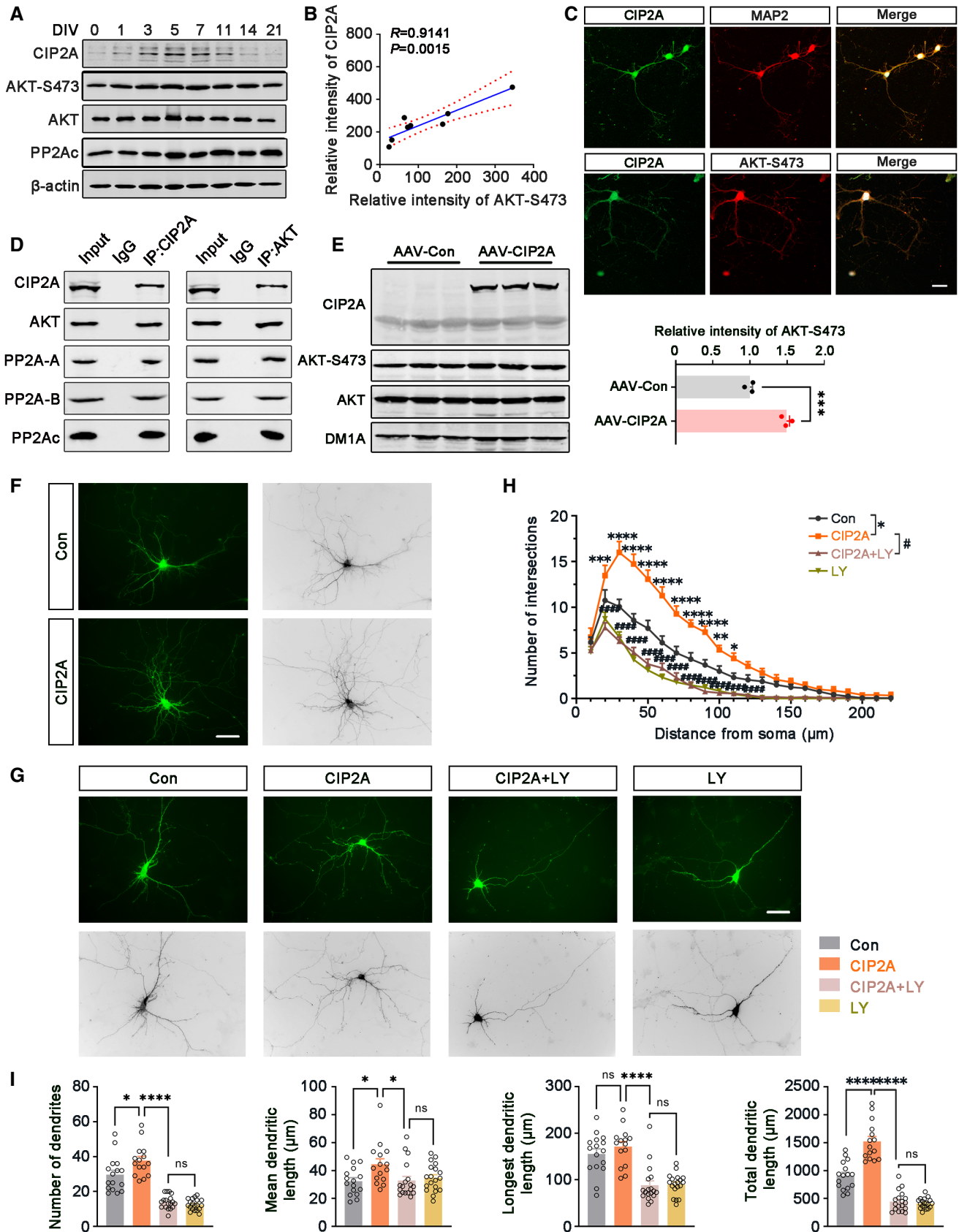


Figure 3.

**Figure 3. CIP2A activates AKT in primary neurons and promotes dendritic development through PI3K-AKT pathway.**

- A Representative immunoblots of CIP2A, AKT-S473, AKT, PP2Ac, and  $\beta$ -actin in primary cortical neurons at DIV 0, 1, 3, 5, 7, 11, 14, and 21. Data represent  $N = 3$  independent experiments.
- B Correlation analysis of AKT-S473 and CIP2A in (A),  $R = 0.9141$ ,  $P = 0.0015$ .
- C Top: representative immunofluorescence staining of CIP2A (green) and MAP2 (red) in the cultured primary hippocampal neurons at DIV 6. Bottom: representative immunofluorescence staining of CIP2A (green) and AKT-S473 (red) in the cultured primary neurons at DIV 6. Scale bar: 20  $\mu$ m.
- D The interaction of CIP2A, AKT, PP2A-A, PP2A-B, and PP2Ac was revealed by Co-IP in cortical neurons (DIV 7). Data represent  $N = 3$  independent experiments.
- E Cultured cortical primary neurons were infected with control or CIP2A-AAV at DIV 5 for 3 days. Representative immunoblots of CIP2A, AKT-S473, AKT, and DMIA (Left) and the quantitative analysis of AKT-S473 (Right).
- F Cultured primary hippocampal neurons were transfected with Surface-EGFP plasmid or Surface-EGFP and CIP2A plasmid at DIV 4. Representative fluorescence images of the neurons at DIV 7. Scale bar: 25  $\mu$ m.
- G Primary cultured hippocampal neurons were transfected with surface-EGFP or surface-EGFP and CIP2A plasmid at DIV 4, with or without LY294002 treatment for 3 days. Representative fluorescence images of neurons at DIV 7 of the four groups. Scale bar: 25  $\mu$ m.
- H Sholl analysis of dendritic arborization of neurons in (G).
- I Quantification of dendritic number, mean dendritic length, longest dendritic length, and total dendritic length of the neurons in (G).

Data information: Data are presented as mean  $\pm$  SEM. ns, not significant; \* $P < 0.05$ , \*\* $P < 0.01$ , \*\*\* $P < 0.001$ , \*\*\*\* $P < 0.0001$ , \*\*\*\*\* $P < 0.00001$ . For (E), AAV-Con  $n = 3$ , AAV-CIP2A  $n = 3$ ,  $n$  represents biological replicates. For (H) and (I), Con  $n = 16$ , CIP2A  $n = 15$ , CIP2A + LY  $n = 18$ , LY  $n = 19$  neurons from three biological replicates for each group. For (E), data are analyzed by Student's  $t$ -test. For (H), data are analyzed by two-way repeated-measures ANOVA followed by Bonferroni's *post hoc* test compared with the con group (\*) or CIP2A + LY group (#). For (I), data are analyzed by one-way repeated-measures ANOVA. Source data are available online for this figure.

**CIP2A knockdown inhibits dendritic growth and AKT activation, which is rescued by overexpression of AKT or active PI3K**

To further confirm the role of CIP2A in the development of dendrite, we downregulated CIP2A in primary neurons to observe whether CIP2A deficiency can block dendritic growth. Primary hippocampal neurons were transfected with CIP2A-ShRNA plasmid with or without co-transfection of AKT plasmid at DIV 2. The knockdown efficiency of CIP2A-ShRNA was confirmed by Western blotting (Fig EV2A–D). The dendritic development was evaluated at DIV 6. Immunofluorescence staining showed that CIP2A deletion induced a marked reduction in the fluorescence intensity of AKT-S473, indicating that CIP2A knockdown inhibited AKT activity (Fig 4A and B). With AKT inhibition, the complexity of dendrite, the number of dendritic branches, the longest dendritic length and the total dendritic length were all significantly decreased compared with the control group (Fig 4C–G). AKT overexpression in CIP2A knockdown neurons reversed AKT inhibition and the impaired dendritic development (Fig 4C–G). Overexpression of AKT increased the phosphorylation of AKT-S473 slightly compared with the control group, but the development of dendrites was not further enhanced (Fig 4). We also overexpressed active PI3K in CIP2A knockdown neurons using the same strategy and observed the similar results (Fig EV3A–G). These data collectively confirm that CIP2A is upstream of AKT-mediated dendritic arborization and development.

**PP2A mediates the effect of CIP2A on AKT activation and dendritic development**

Our findings indicate that CIP2A promotes dendritic arborization/development through interacting with and activating AKT. As an endogenous inhibitor of PP2A, CIP2A regulates protein phosphorylation through inhibiting the dephosphorylation activity of PP2A on specific substrates. AKT on the contrary is an established substrate of PP2A (Andrabi et al, 2007). Next, to confirm the role of PP2A in mediating the regulation of CIP2A on AKT in dendritic development, we overexpressed CIP2A plasmids in N2a cells, with or without co-expression of PP2A catalytic subunit. The results showed that PP2A

overexpression reversed the increased phosphorylation of AKT-S473 caused by CIP2A (Fig 5A and B). Further investigation on primary neurons revealed that overexpression of PP2A reversed the enhanced development of dendrites by CIP2A (CIP2A vs. CIP2A + PP2A, Fig 5C–E). When PP2A was overexpressed and over-activated, CIP2A overexpression was unable to effectively inhibit PP2A, thus induce AKT activation, and promote dendritic development (PP2A vs. CIP2A + PP2A, Fig 5C–E), indicating that PP2A is downstream of CIP2A in regulating dendrite branching. These results also support that CIP2A mainly exerts its regulation on PP2A-AKT signaling in dendritic development under physiological conditions. Overall, these data support that CIP2A participates in dendritic development through PP2A-AKT signaling pathway.

**CIP2A deficiency-induced depression-like behaviors and dendrite/spine loss are rescued by AKT activation**

We have shown that the deletion of CIP2A in mice can cause depression-like behaviors, and CIP2A knockdown in primary neurons inhibits dendritic development and AKT activation. Next, we further explored whether AKT activation can rescue the CIP2A deficiency-induced depression *in vivo*. For this purpose, we injected AAV-SiCIP2A or AAV-AKT(S473E)-SiCIP2A virus into the bilateral ventricles of newborn C57/BL6 mice (postnatal day 2–4) to knockdown CIP2A, with or without simultaneously activating AKT (Fig 6A and B). The efficient knockdown of CIP2A and overexpression of AKT were confirmed by Western blotting using brain hippocampal tissues after 2 months (Fig EV4A–D). Before sacrificing the mice, we performed relevant behavioral tests to evaluate the depression-like phenotypes. In open field test, the center distance (m) was significantly decreased in SiCIP2A mice compared with control mice, while AKT activation increased the center distance (m) and the time in center (s) in SiCIP2A mice (Fig 6C–E), indicating that CIP2A deficiency-induced anxiety can be rescued by active AKT. In sucrose preference test, SiCIP2A mice showed decreased tendency of sucrose preference ratio (%), while AKT activation could significantly increase the sucrose preference ratio (%) in SiCIP2A mice (Fig 6F). Depression-like behaviors like decreased

social-interaction time in three-chamber social approach task, and decreased struggling time (s) and increased immobility time (s) in tail suspension test, were observed in SiCIP2A mice, which were all

rescued by AKT activation (Fig 6G–I). The results demonstrate that CIP2A deficiency-induced AKT inhibition plays a key role in promoting depression in mice.

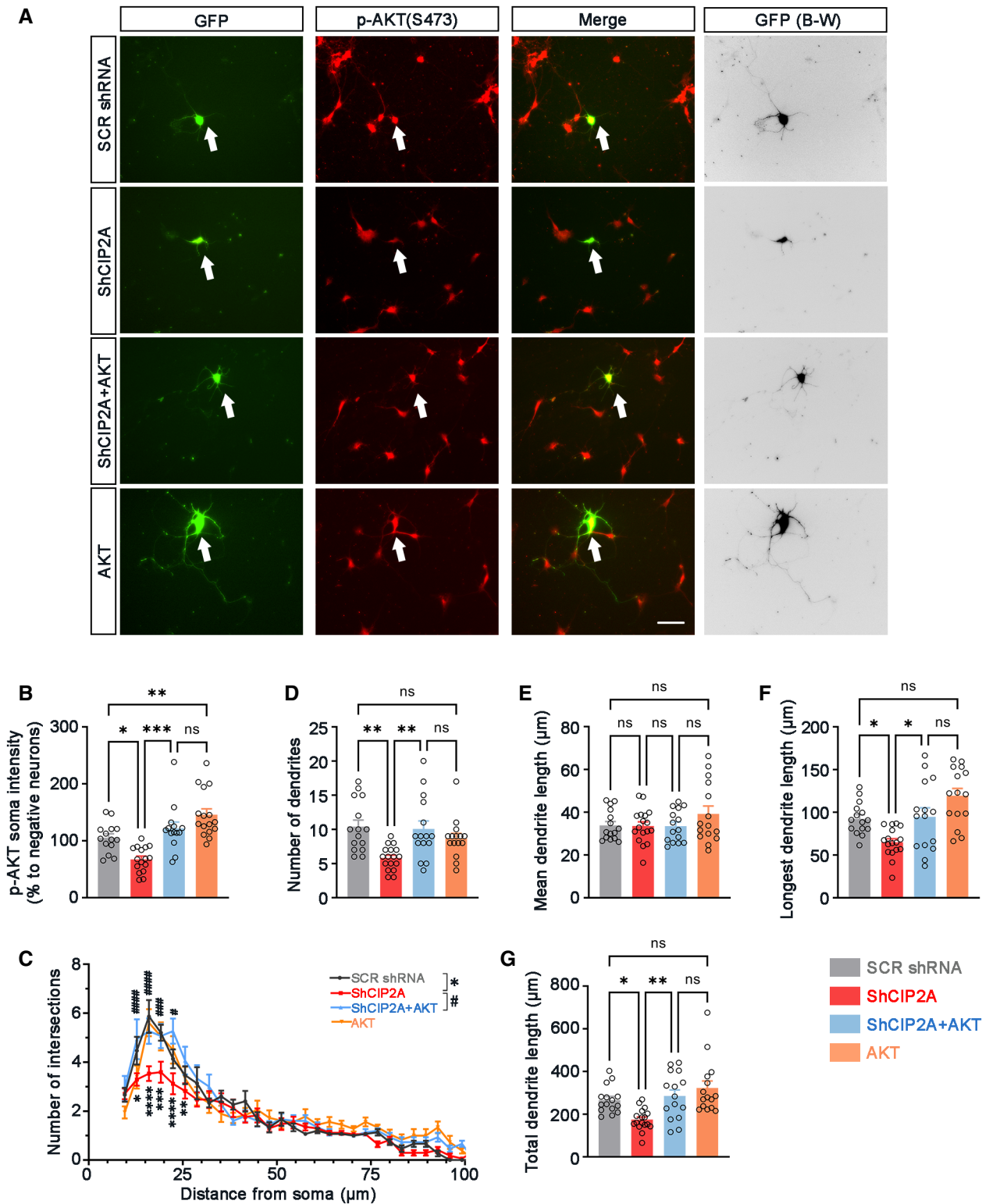


Figure 4.



**Figure 4. CIP2A knockdown inhibits dendritic growth and AKT activation, which is rescued by replenishing AKT.**

SCR (scramble) plasmid, CIP2A-shRNA plasmid, CIP2A-shRNA plasmid + AKT plasmid or AKT plasmid were overexpressed together with Surface-EGFP plasmid in cultured primary hippocampal neurons at DIV 2. Neuronal morphology (green) was observed on DIV 6.

A Representative fluorescence images of GFP (green) and AKT-S473 (red) in the cultured primary hippocampal neurons at DIV 6 of the four groups. Arrows in CIP2A-shRNA group show a CIP2A knockdown neuron has markedly reduced AKT-S473 signal, and the dendritic development is severely impaired; Arrows in CIP2A-shRNA+AKT group show that AKT transfection successfully rescues AKT-S473 phosphorylation and the dendritic development. B-W: black in white background GFP image; scale bar: 25  $\mu$ m.

B Quantitative analysis of the fluorescence intensity of AKT-S473 immunostaining.

C Sholl analysis of dendritic arborization of the neurons in (A).

D–G Quantification of dendritic number (D), mean dendritic length (E), longest dendritic length (F), and total dendritic length (G) of hippocampal neurons in (A).

Data information: Data are presented as mean  $\pm$  SEM. ns, not significant; \* $P$  < 0.05, \*\* $P$  < 0.01, \*\*\* $P$  < 0.001, \*\*\*\* $P$  < 0.0001, # $P$  < 0.05, ### $P$  < 0.001, ##### $P$  < 0.0001. For (B), SCR-shRNA  $n$  = 14, CIP2A-shRNA  $n$  = 16, CIP2A-shRNA+AKT  $n$  = 14, AKT  $n$  = 16 neurons from three biological replicates for each group. For (C–G), SCR-shRNA  $n$  = 15, CIP2A-shRNA  $n$  = 17, CIP2A-shRNA+AKT  $n$  = 15, AKT  $n$  = 15 neurons from three biological replicates for each group. For (C), data are analyzed by two-way repeated-measures ANOVA followed by Bonferroni's *post hoc* test compared with the SCR-shRNA group (\*) or CIP2A-shRNA+AKT group (#). For (B) and (D–G), data are analyzed by one-way repeated-measures ANOVA.

Next, we further explored whether CIP2A deficiency-induced defect in dendritic arborization could be rescued by activating AKT. Golgi staining of the hippocampal neurons showed that the complexity of dendrite was significantly reduced in SiCIP2A mice compared with control mice, which was partially reversed by AKT activation (Fig 6J and K). In addition, the decreased number of dendritic branches, mean dendritic length, and total dendritic length in SiCIP2A mice were all reversed by overexpressing active AKT (Fig 6L–O). CIP2A deficiency did not induce neuron loss (Fig EV5A and B). However, it induced a significant loss of synapse manifested by decreased spine numbers, which was rescued by AKT activation (Fig 6P and Q). Similar to the results in cultured neurons, overexpression of AKT alone, though slightly increased AKT activity (Fig EV4D), did not further promote dendrite growth compared with control, indicating that excessive AKT activation is not beneficial for dendrite development. Overall, these data support that the defect in AKT-mediated dendrite branching/spine development is a key event in CIP2A deficiency-induced depression.

**Decreased CIP2A expression and impaired dendritic arborization in CUMS depression rat models**

To further verify the involvement of CIP2A in the pathogenesis of depression, we examined the expression of CIP2A and dendritic arborization/spine development in other animal models of depression. Chronic unpredictable mild stress (CUMS) model is a well-established

animal model of depression. Depression-like behaviors and deficits in synaptic plasticity are gradually developed during CUMS (Willner *et al*, 1987; Qiao *et al*, 2014). Moreover, the CUMS model recapitulates many of the core behavioral characteristics of human depression (Willner, 2005; Hill *et al*, 2012). We therefore examined the protein levels of CIP2A and the active form of AKT (AKT-S473) in the hippocampal tissues of CUMS rat models. Western blotting results showed that the levels of CIP2A and active AKT (AKT-S473) were decreased in CUMS model (Fig 7A–C). Golgi staining revealed that the hippocampal neurons in CUMS rat brains had impaired dendritic arborization/synaptic development compared with the control group, which were manifested by decreased dendritic complexity, reduced dendritic branches number, decreased mean dendritic length, longest dendritic length and total dendritic length, and reduced density of spines (Fig 7D–K). These data validate the correlation of low brain CIP2A levels with depression onset in rodents and further support the role of CIP2A-dependent defects in brain plasticity in the development of depression.

**Discussion**

Major depression disease is a devastating disease with limited treatment strategies at current (Fava, 2003; Holtzheimer & Mayberg, 2011; Ledford, 2014; McIntyre *et al*, 2014). Development of effective therapies depends on the discovery of key disease

**Figure 5. PP2A mediates the effect of CIP2A on AKT activation and dendritic development.**

A N2a cells were transfected with vector, CIP2A, CIP2A + PP2A or PP2A plasmids for 48 h. Representative immunoblots of AKT-S473, AKT, CIP2A, PP2Ac and  $\beta$ -actin of the four groups.

B The quantitative analysis of AKT-S473 in (A).

C Primary hippocampal neurons were transfected with vector, CIP2A, CIP2A + PP2A or PP2A plasmids at DIV 4. Representative fluorescence images of the neurons at DIV 7. Scale bar: 25  $\mu$ m.

D Sholl analysis of dendritic arborization of the neurons in (C).

E Quantification of dendritic number, mean dendritic length, longest dendritic length, and total dendritic length of hippocampal neurons in (C).

Data information: Data are presented as mean  $\pm$  SEM. ns, not significant; \* $P$  < 0.05, \*\* $P$  < 0.01, \*\*\* $P$  < 0.001, \*\*\*\* $P$  < 0.0001, ## $P$  < 0.01, #### $P$  < 0.001, ##### $P$  < 0.0001. For (B),  $n$  = 3 per group,  $n$  represents biological replicates. For (D, E), Con  $n$  = 16, CIP2A  $n$  = 15, CIP2A + PP2A  $n$  = 18, PP2A  $n$  = 19 neurons from three biological replicates for each group. For (D), data are analyzed by two-way repeated-measures ANOVA followed by Bonferroni's *post hoc* test compared with the con group (\*) or CIP2A + PP2A group (#). For (B) and (E), data are analyzed by one-way repeated-measures ANOVA.

Source data are available online for this figure.

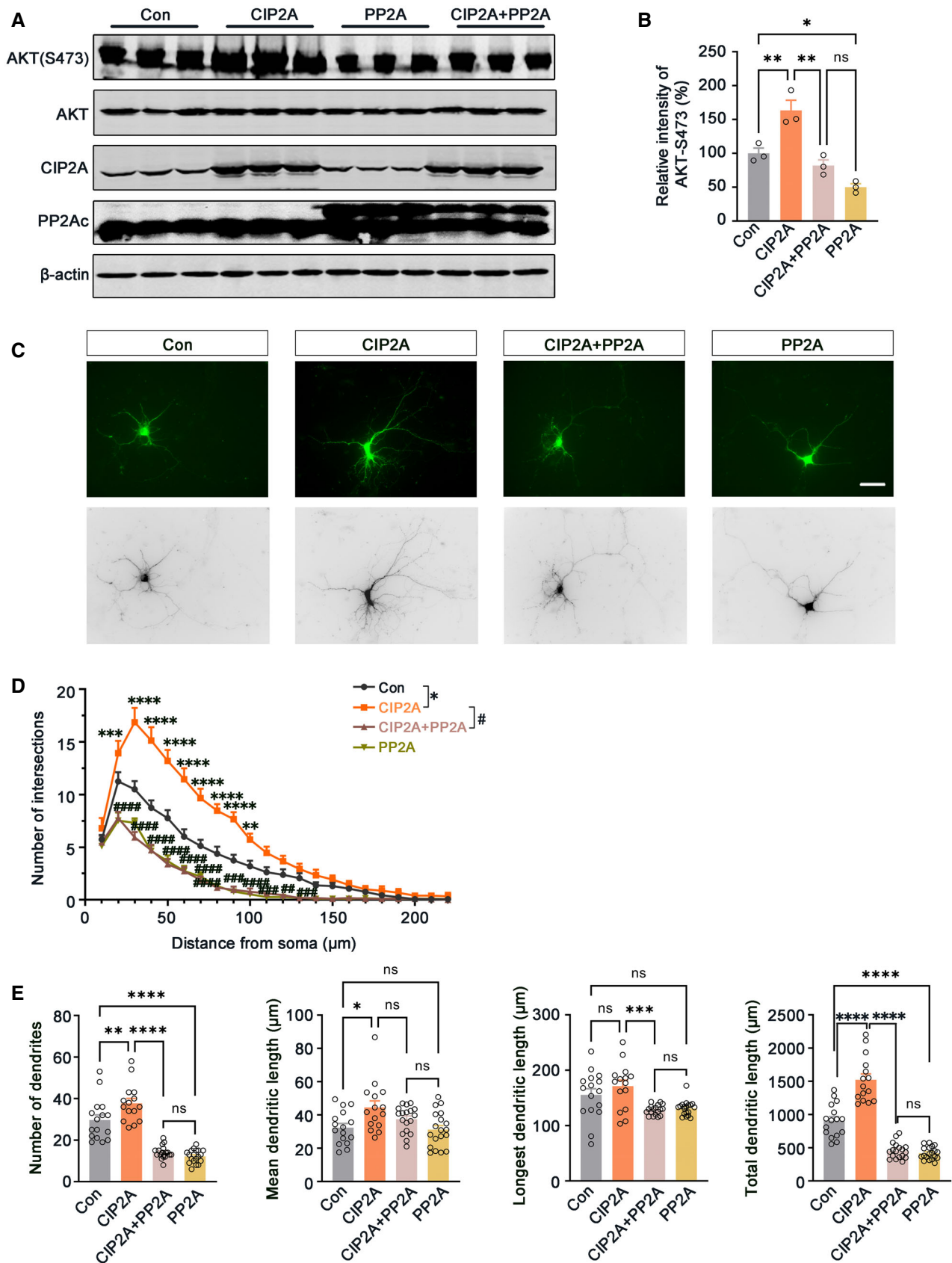


Figure 5.

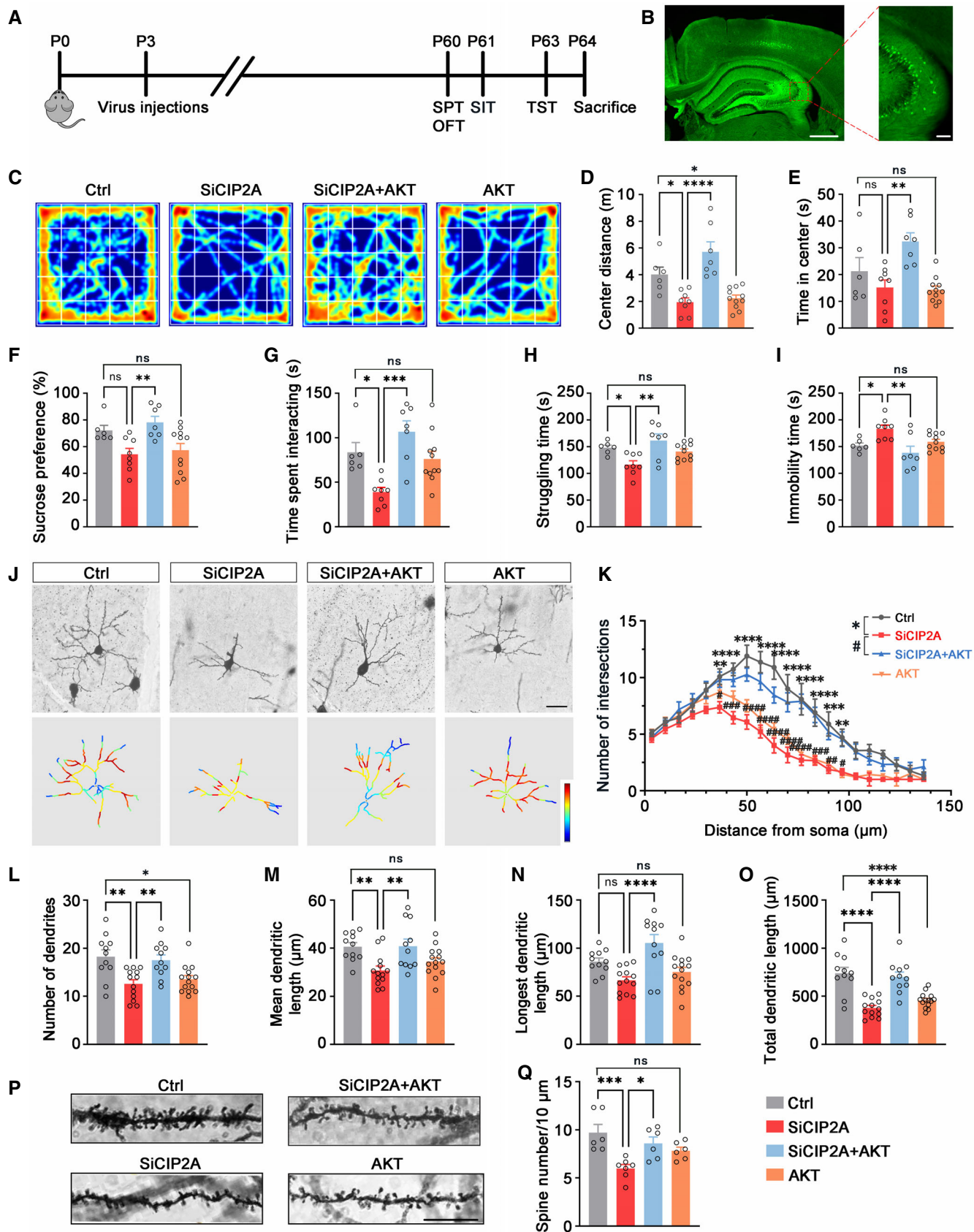


Figure 6.

**Figure 6. CIP2A deficiency-induced depression-like behaviors and defect in dendrite arborization/spine development are rescued by AKT activation.**

Newborn mice (postnatal 2–4 days) were divided into four groups and injected with AAV-Con, AAV-SiCIP2A, AAV-AKT(S473E)-SiCIP2A or AAV-AKT(S473E) virus, respectively, into the bilateral ventricles. After 2 months, all mice were tested by different behavioral test paradigms and brains were collected for Golgi staining. The same cohort of mice was used for each behavioral test.

A Experimental timelines for virus stereotaxic injections and behavioral tests.

B The representative fluorescence image confirms the expression of virus. Scale bar: 500  $\mu\text{m}$  (left panel) and 100  $\mu\text{m}$  (right panel).

C–E The representative searching trace (C), the distance in center (m) (D) and the time in center (s) (E) in open field test of the mice in four groups.

F The sucrose preference ratio (%) of the mice in four groups.

G The time spend in interacting (s) with another mouse in three-chamber sociability test.

H, I The struggling time (s) (H) and the immobility time (s) (I) in tail suspension test of the mice in four groups.

J Representative Golgi staining images of hippocampal neurons of the mice in four groups (Top). Neuronal morphology tracings of Golgi-stained neurons (Bottom). Scale bar: 25  $\mu\text{m}$ .

K Sholl analysis of dendritic arborization of the neurons in (J).

L–O Quantification of dendritic number (L), mean dendritic length (M), longest dendritic length (N), and total dendritic length (O) of hippocampal neurons in (J).

P Representative Golgi staining images of the spines in hippocampal neurons. Scale bar: 10  $\mu\text{m}$ .

Q The quantitative analysis of the spine number in (P).

Data information: Data are presented as mean  $\pm$  SEM. ns, not significant; \* $P < 0.05$ , \*\* $P < 0.01$ , \*\*\* $P < 0.001$ , \*\*\*\* $P < 0.0001$ , # $P < 0.05$ , ## $P < 0.01$ ,

### $P < 0.001$ , #### $P < 0.0001$ . For (D–I), Control  $n = 6$ , SiCIP2A  $n = 8$ , AKT(S473E)-SiCIP2A  $n = 7$ , AKT(S473E)  $n = 11$ ,  $n$  represents biological replicates. For (K–O),

Control  $n = 11$ , SiCIP2A  $n = 13$ , AKT(S473E)-SiCIP2A  $n = 11$ , AKT(S473E)  $n = 14$  neurons from three biological replicates for each group. For (Q), Control  $n = 6$ ,

SiCIP2A  $n = 7$ , AKT(S473E)-SiCIP2A  $n = 6$ , AKT(S473E)  $n = 6$  spines from three biological replicates for each group. For (K), data are analyzed by two-way

repeated-measures ANOVA followed by Bonferroni's *post hoc* test compared with the con group (\*) or AKT(S473E)-SiCIP2A group (#). For (D–I), (L–O) and (Q),

data are analyzed by one-way repeated-measures ANOVA.

mechanisms. In the present study, we disclose the role of CIP2A in regulating neuronal plasticity through ATK signaling and report that CIP2A deficiency may underlie the pathogenesis of depression. Our findings reveal a new molecular regulating pathway involved in the pathophysiology of depression.

In our study, the role of CIP2A deficiency in promoting depression development was identified in several animal models. First, CIP2A knockout mice showed typical anxiety- and depression-like behaviors in a series of behavioral tests. Similar results were observed in CIP2A knockdown mice in which brain CIP2A expression was inhibited by CIP2A-ShRNA *in vivo*. Furthermore, in a classic CUMS depression model, brain CIP2A levels were decreased significantly compared with control. At last, in clinical MDD patients, CIP2A expression levels in brain cortex showed a tendency of decrement ( $P = 0.06$ ). All these data suggest that CIP2A dysregulation may play a role in depression.

Currently, researchers raise a lot of hypotheses to explain the pathogenesis of depression. A defect in brain plasticity, which is manifested by neuronal atrophy and synaptic loss, is consistently found in MDD patients and animal models (Conrad, 2008; David et al, 2009; He et al, 2021) and is supposed to be an important pathology underlying depression phenotype. Key events of brain plasticity include the establishment and maintenance of dendrite branching complexity, as well as synaptogenesis. Through a global gene expression screen and analysis in CIP2A knockout mice, we focus our attention to the impaired dendritic arborization/development in the development of depression in CIP2A-deficient mice. Our data show that CIP2A knockdown induces retarded dendritic development in cultured primary neurons and decreased dendritic arborization/growth and synaptogenesis in animal brains. In CUMS depression model, decreased CIP2A expression is coincident with the occurrence of dendritic arborization and synaptic development deficits. In addition, the CIP2A expression is highly related to dendritic development in cultured neurons, and CIP2A overexpression remarkably enhances dendritic growth. These data strongly indicate that CIP2A is an important molecular regulator of dendritic

development, and defect of this regulation participates in CIP2A deficiency-induced depression.

CIP2A is an endogenous inhibitor of PP2A, which exert its biological function through regulating the phosphorylation of PP2A substrates (Junttila et al, 2007). AKT is a PP2A dephosphorylation target. With PP2A dephosphorylating the key enzyme activity-regulatory site Ser473, AKT is inhibited (Vauzour et al, 2018). Reversely, when PP2A is inhibited by some factors such as endogenous inhibitors, AKT may be activated. Furthermore, AKT has been identified as an important kinase in promoting neurite growth (Atwal et al, 2000; Markus et al, 2002), and CIP2A can positively regulate AKT activity in tumor cells (Chen et al, 2010; Gao et al, 2020). Relating to depression, activation of PI3K-AKT signaling was found to play an antidepressant role, and inhibition of AKT signaling pathway could promote the development of depression in rodents (Li et al, 2020; Jiang et al, 2021; Wang et al, 2021). In our study, the transcriptome data from both CIP2A knockdown mice and MDD patients indicate that PI3K-AKT signaling is one of the mainly influenced signaling pathways. Based on the transcriptome analysis result and related published reports, we suspect that dysregulated PP2A-AKT signaling is a key event in the impaired dendritic arborization/growth and synaptogenesis induced by CIP2A deficiency. This hypothesis is confirmed by our *in vivo* and *in vitro* experiments. First, CIP2A interacts with AKT and PP2A in dendrites and positively regulates AKT activity in neurons during the development. In CUMS depression model, with CIP2A downregulation, AKT activity is also reduced. Second, in cultured neurons, CIP2A overexpression promotes dendritic development, which is blocked by PI3K inhibitor; CIP2A knockdown results in retarded dendritic arborization, which can be rescued by AKT or active PI3K. Third, in mice, CIP2A knockdown in the brain induces impairment of dendritic arborization/development and synaptogenesis, which is able to be rescued by overexpressing active AKT. At last, PP2A overexpression reverses CIP2A-induced AKT activation and enhancement of dendritic growth. All these results suggest that CIP2A deficiency induces

impaired neuronal plasticity through inhibition PP2A-AKT signaling pathway.

Taking together, our data indicate that CIP2A participates in dendritic arborization through PP2A-AKT signaling pathway, and CIP2A deficiency underlies depression development through impairing AKT-mediated neuronal plasticity.

Although our results showed that the CIP2A-PP2A-AKT signaling pathway was involved in the development of dendrites and the pathogenesis of depression, the upstream factors of CIP2A deficiency still need to be further explored. Through GWAS analyzing,

we did not find *CIP2A* gene mutations in MDD patients (Wray et al, 2018; Howard et al, 2019), indicating that decreased CIP2A expression may result from other upstream undisclosed factors. Moreover, the impact of CIP2A deficiency on synaptic plasticity requires further investigation.

In conclusion, CIP2A participates in the development of dendrites through CIP2A-PP2A-AKT signaling pathway. Defect in CIP2A-PP2A-AKT pathway participates in the development of depression. Our study discloses a new mechanism of depression and a possible new direction for depression treatment in clinical research.

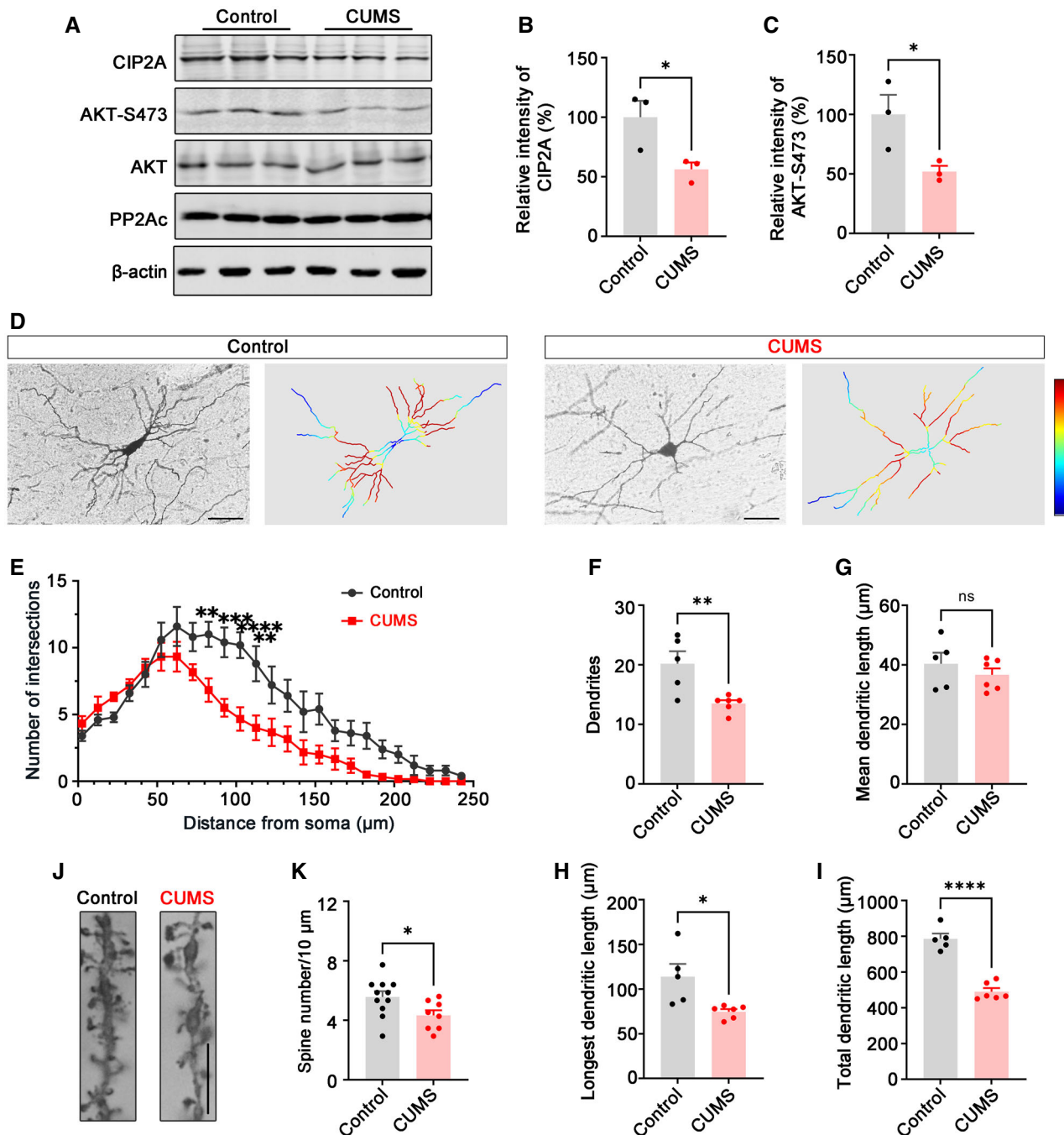


Figure 7.

**Figure 7. Decreased CIP2A expression and impaired dendritic arborization in CUMS model.**

- A Representative immunoblots of CIP2A, AKT-S473, AKT, PP2Ac and  $\beta$ -actin of brain tissue homogenates from hippocampus of the control and CUMS rats.  
 B, C The quantitative analysis of CIP2A (Left) and AKT-S473 (Right) in (A).  
 D Representative Golgi staining images of neurons in the hippocampus of control and CUMS rats (Left). Neuronal morphology tracings of Golgi-stained neurons (Right). Scale bar: 25  $\mu$ m.  
 E Sholl analysis of dendritic arborization of the neurons in (D).  
 F–I Quantification of dendritic number (F), mean dendritic length (G), longest dendritic length (H), and total dendritic length (I) of hippocampal neurons in (D).  
 J Representative Golgi staining images of the spines in hippocampal neurons. Scale bar: 10  $\mu$ m.  
 K The quantitative analysis of the spine number in (J).

Data information: Data are presented as mean  $\pm$  SEM. ns, not significant; \* $P$  < 0.05, \*\* $P$  < 0.01, \*\*\* $P$  < 0.001, \*\*\*\* $P$  < 0.0001. For (B–C),  $n$  = 3 mice per group,  $n$  represents biological replicates. For (E–I), Control  $n$  = 5, CUMS  $n$  = 6 neurons from three biological replicates for each group. For (K), Control  $n$  = 11, CUMS  $n$  = 8 spines from three biological replicates for each group. For (E), data are analyzed by two-way repeated-measures ANOVA followed by Bonferroni's *post hoc* test. For (B, C), (F–I) and (K), data are analyzed by Student's *t*-test.

Source data are available online for this figure.

## Materials and Methods

### Antibodies and plasmids

The primary and secondary antibodies used in this study were as follows: anti-CIP2A (sc-80662, Santa Cruz), anti-CIP2A (A12267, Abclone), anti-MAP2 (AB5622, Millipore), anti-AKT (9272 S, Cell Signaling Technology), anti-AKT (2967 S, Cell Signaling Technology), anti-AKT-S473 (4060 S, Cell Signaling Technology), PP2Ac (05-421, Millipore), anti-PP2Ac (R25422, Zenbio), anti-PP2A-B (16569-1-AP, Proteintech), anti-PP2A-A (12621-1-AP, Proteintech), anti-DM1A (04-1117, Millipore), anti- $\beta$ -actin (66009-1-Ig, Proteintech), anti-mouse IgG (12-371, Millipore), Alexa Fluor 488 donkey anti-mouse (715-546-151, Jackson Immuno Research Labs), Alexa Fluor<sup>®</sup> 594 AffiniPure Donkey Anti-Rabbit IgG (715-585-152, Jackson Immuno Research Labs), and LY294002 (HY-10108, MCE). CIP2A and ShRNA-CIP2A plasmids were from Neuron Biotech (Shanghai, China), PP2Ac plasmid was from Dr. Haendeler (University of Frankfurt, Germany), and PI3K and AKT plasmids were constructed in H.Y.M's laboratory.

### Animals

C57B6/L mice were obtained from the Experimental Animal Center of Tongji Medical College, Huazhong University of Science and Technology. CIP2A knockout mice were provided by JW, and the related information has been published previously (Ventelä *et al.*, 2012). In our study, 6-month-old male CIP2A knockout mice and the age-matched male WT C57B6/L mice were used. For AAV virus infection, newborn C57B6 mice (male and female) were used. All animals were kept in a condition with appropriate temperature (22  $\pm$  2°C), humidity (55  $\pm$  15%) and 12–12-h light–dark cycle, and had continual access for food and water freely. Mice were assigned to experimental groups using simple randomization in a manner that assured age matching between experimental conditions. All animal experiments were approved by the Animal Care and Use Committee of Huazhong University of Science and Technology and performed in compliance with the NIH Guide for the Care and Use of Laboratory Animals.

### Cell culture and treatment

For N2a cells, cells were cultured in DMEM-high glucose medium containing 10% fetal bovine serum (Gibco BRL, Gaithersburg, MD,

USA) in a humidified incubator aerated with 95% air and 5% CO<sub>2</sub> at 37°C. The cells were seeded into 6-well plates and changed to fresh medium when the confluence reached to 70–80% and then transfected with relevant plasmids by Neofect DNA transfection reagent according to the manufacturer's protocols (Neofect Biological Technology, Beijing, China). Cells were collected for subsequent experiments 48-h posttransfection.

For primary neurons, hippocampal and cortex tissues were isolated from embryos (E15–E18) of Sprague–Dawley rats. Hippocampal neurons were used for imaging due to their better morphology, and cortical neurons were used for Western blotting and co-immunoprecipitation (Co-IP). Tissues were cleaned with D-hanks and incubated with 0.25% trypsin for 20 min and then titrated through a 40- $\mu$ m cell filter to obtain single cells. The cell suspension was resuspended with planting medium containing MEM/F12 with 10% fetal bovine serum to terminate the digestion. Then, the cell suspension was seeded onto plates, which were coated with poly-D-lysine and incubated in incubator at 37°C in the presence of 5% CO<sub>2</sub>. After 4–6 h, the planting medium was replaced with neurobasal medium supplemented with 2% B-27, 1% GlutaMAX (2 mM), 1% penicillin (50 U/ml) and streptomycin (50  $\mu$ g/ml). During the culture, the medium was half-changed every 3 days with fresh maintenance medium.

For immunofluorescence imaging, the primary neurons were transfected with relevant plasmids by Lipofectamine<sup>™</sup> 2000 transfection reagent according to the manufacturer's protocols (Lipofectamine 2000 Transfection Reagent, Thermo Fisher Scientific, USA). Cells expressing EGFP were observed under a confocal microscope (LSM710, Zeiss, Germany). For immunoblotting, primary neurons were infected with control or CIP2A-AAV for 48 h and cells were then collected and lysed for subsequent experiments.

### Western blotting and Co-IP

Cell samples and brain tissue were lysed or homogenized with RIPA buffer (Beyotime Biotechnology, Shanghai, China) containing PMSF (1:100) and proteinase inhibitor cocktail (1:100), then boiled for 10 min, and centrifuged at 14,000 *g* for 10 min. The supernatants were collected, and protein concentrations were quantified by BCA kit (Thermo Fisher Scientific, Waltham, Massachusetts, USA). The proteins in the extracts were separated by 10% SDS–PAGE and transferred to nitrocellulose membrane. Then, the membranes were blocked with 5% nonfat milk for 1 h and incubated with primary

antibodies overnight at 4°C. Then, the membranes were washed for three times with TBST for 10 min each and incubated with the secondary antibody at room temperature for 1 h in dark. Blots were visualized using the Odyssey Infrared Imaging System (Li-Cor Biosciences, Lincoln, NE, USA). The protein bands were quantitatively analyzed by ImageJ software (Rawak Software, Germany).

To analyze protein–protein interactions, we performed co-immunoprecipitation (Co-IP) using cell lysates. The extracts (about 200 mg total proteins) were incubated with specified antibodies and protein G at 4°C overnight. The agarose beads were collected and washed three times with PBS. Last, the sediment was resuspended with 2× loading buffer, and boiled for 5 min, the bound proteins were analyzed by Western blotting.

### Immunofluorescence and fluorescence imaging

For immunofluorescence, neurons were washed with PBS buffer and then fixed with 4% paraformaldehyde (PFA) for 10 min, permeabilized in 0.5% Triton X-100 for 10 min, and followed by incubation with 3% BSA to block nonspecific sites. Next, the cells were incubated with primary antibodies overnight at 4°C. After washing, the sections were incubated with Alexa 488- and 594-conjugated secondary antibodies for 1 h, mounted and air-dried in dark. For observation of the cell morphology, neurons cultured on round slips were fixed, and EGFP-expressing cells were observed under the microscope directly. All of the images were observed with the LSM710 confocal microscope (Zeiss, Germany).

### Stereotaxic injection

C57B6 mice pups at postnatal day 2 were anesthetized on ice for 3 min. Then, the mice were injected AAV virus into the bilateral ventricles using a specially designed, fine 10 µl Hamilton syringe equipped with a 30G/0.5 inch/hypodermic cemented needle (Hamilton Syringe Company, Reno, NV, USA). Behavioral tests were performed after 2 months. pAAV-SYN-SiCIP2A-EGFP-3FLAG, pAAV-SYN-AKTS473E-2A-EGFP-3FLAG-H1-SiCIP2A and pAAV-SYN-AKTS473E-2A-EGFP-3FLAG were from OBiO technology (Shanghai, China). pAAV-SYN-AKTS473E-2A-EGFP-3FLAG-H1-SiCIP2A infection results in neuronal expression of AKTS473E and SiCIP2A simultaneously. AKTS473E mimics S473-phosphorylated AKT, thus is an AKT active mutant.

### Nissl staining

The mice brain after perfusion and fixation (with 4% formaldehyde) was sliced at 30 µm thickness. The frozen sections were mounted on the slide, and the brain slices were stained according to the manufacturer's procedure (Beyotime Biotechnology, Shanghai, China).

### Golgi staining

The mice were anesthetized by isoflurane, and each mouse was perfused intracardially with 40 ml of normal saline containing 0.5% sodium nitrite. The brains were taken out and soaked in Golgi dye solution containing 5% potassium chromate, 5% mercuric chloride,

and 5% potassium dichromate at room temperature for 20 days in the dark. Then, the brains were serially sectioned into 100 µm thick slices through a vibrating microtome (Leica, VT1000S, Germany). The sections were rinsed in double distilled water for 1 min and then soaked with ammonium hydroxide for 30 min and double distilled water for 1 min in the dark. Next, the slices were dehydrated with increasing gradient of alcohol (50, 70, 95, and 100%) and transferred to a CXA solution containing formyl trichloride, xylene, and absolute ethyl alcohol (1:1:1) for 15 min. Last, the slices were mounted and images were taken using light microscope (Nikon, 90i, Japan).

### Dendrite morphology analysis

ImageJ software was used for dendrite morphology analysis. In brief, the captured neuronal image was converted to grayscale and saved. The saved grayscale image was then opened in ImageJ, and the ruler was set; the “Neuron J” patch was used to trace the dendrites and outline the neuronal structure, and then, the picture was saved. Lastly, open the saved picture again, draw the distance from the cell body to the farthest dendrite, and click “Sholl Analysis” to get the relevant measurements of the neuron dendrites. The data were saved for subsequent analysis.

### Rotarod test

Motor performance was evaluated using a rotarod apparatus with a 3 cm diameter rod (Ugo Basile, Monvalle, Italy) at accelerating rotation rate (10 speeds from 4 to 40 rpm for 5 min). On the day preceding the experiment, all mice were trained on the rotarod at a speed of starting at 4 rpm and were excluded if they did not continue to walk on the rotarod. Then, the mice were detected for three trials, 5 min per trial. The running time and speed were recorded, and the mean latency and speed on the rod were calculated.

### Grip test

Grip test was performed using a wooden pole, which was 20 cm high from the table. During the test, the experimenter held the mice by their tails, allowing the mice to grab the pole using their forepaws, and then recorded the time from releasing the tail to when it fell off. The test was repeated five times per mouse, and the mean time was calculated.

### Footprint assay

The footprint test provides an analysis of motor coordination and balance. Briefly, the fore and hind limbs of the mouse were dyed with red and blue ink, respectively. After that, the mice were allowed to walk on white paper (30 cm in length and 5 cm in width) without constraints and then the footprints were scanned and analyzed. Stride length which assessed limb coordination ability was characterized as the distance between the center of the fore limb and hind limb and the distance between the two steps of hind limb. The distance between hind and hind paws (cm) and the distance between front and hind paws (cm) were recorded.

### Open field test (OFT)

In open field test, the animals were placed in an empty area (50 cm × 50 cm × 50 cm plastic container, Techman Software Co, Ltd, Chengdu, China) for 5 min. The floor was divided into 5 × 5 sectors; we defined the middle 3 × 3 sectors and the rest sectors as “center area” and “peripheral area,” respectively. The area was cleaned with 75% ethanol between each habituation period. The distance of horizontal activity (m) and vertical activity (m), the center distance (m), and the time in center (s) were recorded. Center duration (%) was the ratio of the time in center to total time.

### Sucrose preference test (SPT)

In this experiment, the sucrose preference was tested to assess the responsiveness to positive stimuli. Mice were placed individually into a cage and deprived of water for 12 h. After that, each cage was provided with two bottles of solution with 2% sucrose solution or water, respectively. After 4–6 h, the consumption of sucrose water and clean water during this time period was recorded and the preference of sucrose was calculated as sucrose preference (%) = [(sucrose consumption) / (water consumption + sucrose consumption)] × 100%.

### Forced swim test (FST)

In the forced swim test, mice were placed individually into a plastic transparent container (18 cm diameter and 25 cm height) containing water (25 ± 2°C) to depth of 15 cm, in which there was no way to escape or touch the bottom. The duration of immobility (defined as the length of time in which the animal did not show escape responses) was manually scored during a 6-min session. The mouse was judged to be immobile when it remained in the water without struggling and was making only those movements necessary to keep its head above water. Then, animals were removed from the container and left to dry in a heated enclosure before they were returned to their home cages. The cylinder was emptied, washed, and refilled with new water between mice. Data were collected and analyzed by the software.

### T maze

The maze was constructed from gray plastic. The two goal arms were 25 cm long and 6 cm wide, with 20 cm high walls, and the main arm was 30 cm long and 6 cm wide, with 20 cm high walls. The apparatus was monitored by a video camera positioned above of it. The mice were placed in the narrow chamber at the end of the main arm and were adjusted to the environments for 30 s, and then the experimenter opened the baffle. The number of probes on two goal arms and the final position of the mice were monitored. The entrance times of the two goal arms were recorded. The procedure was repeated until a total of seven trials were obtained of each mouse. Between animals, the maze was thoroughly cleaned using 70% ethanol and carefully dried thereafter. The change times were recorded if the mice chose to enter the other arm.

### Morris water maze test (MWM)

Spatial learning and memory were detected by Morris water maze (MWM, Techman Software Co., Ltd., Chengdu, China). The MWM task was performed as previously described. A circular pool (1.2 m in diameters and 50 cm in height) was filled with nontransparent water (23 ± 2°C), and an escape platform was placed 1.5 cm below the water surface at a fixed position in a target quadrant. The test contains acquisition training and probe trial. Before the test began, the mice were habituated to the behavior room and trained on the five consecutive days, three trials per day. During the acquisition training, the mice were put into the pool from different starting points each trial of a daily training session to find the hidden platform. The mice have up to 60 s to find the hidden platform; otherwise, it would be guided to the platform and stayed on it for 20 s. Latency time (s) to find the hidden platform was recorded after each trial of each learning session for 5 consecutive days. On the seventh day, the hidden platform was removed and the mice were placed into the pool for the probe trial for 60 s. The number of times to cross the position of the platform was recorded.

### Tail suspension test (TST)

In this test, the rear 1/3 of the tail of the mouse was fixed with tape and hung on a bracket; the head was away from the table about 15 cm. All animals were suspended for 6 min in total; the behavioral parameters including immobility time (defined as the absence of any body or limb movements except for those caused by respiration) and struggling time during the last 5 min were recorded in seconds.

### Three-chamber social test

The three-chamber test for sociability and social novelty preference was performed as previously described (Buffington *et al*, 2016). Briefly, the device was a 60 × 40 cm<sup>2</sup> box divided into three equally sized, interconnected chambers (left, center, and right). During the adaptation period, the mice were put into the starting area—the middle box and explored on the box freely for 10 min to adapt to the environment. At the end of the session, the mouse was transferred to an empty cage and the experimental area was cleaned with 75% ethanol. In the second 10 min, sociability was measured. During this period, the subject could interact either with an empty mesh cylinder in the left chamber or the sex-matched stranger mouse stayed in another mesh cylinder in the right chamber, and the cylinders allowed for visual and olfactory exchange. The time spent interacting with the stranger was recorded.

### Transcriptomics procedures

The mice were anesthetized by isoflurane, and each mouse was perfused intracardially with normal saline. Hippocampal tissue of mice was isolated, and total RNA was extracted using Trizol Reagent. After that, magnetic beads with Oligo(dT) were used to enrich eukaryotic mRNA (if it is prokaryotic, use the kit to remove rRNA and go to the next step). For the extracted eukaryotic mRNA, fragmentation buffer was added to break the mRNA into short fragments as the templates for synthesizing the first cDNA strand with



random hexamer primers. Then, dNTPs, RNase H, and DNA polymerase I were added to induce the synthesis of the second strand. The cDNA chain was purified by QiaQuick PCR kit and eluted with EB buffer, and then end-repaired and poly(A) added, and the sequencing adapter was connected. Next, agarose gel electrophoresis was used for fragment size selection, and finally, PCR amplification was performed. The constructed sequencing library was sequenced with Illumina HiSeq™. Samples are sequenced on the platform to get image files, which are transformed by the software on the sequencing platform, and the original data in FASTQ format (Raw Data) are generated. The filtered reads were mapped to the reference genome using HISAT2 v2.1.0. The differentially expressed gene (DEG) analysis was analyzed by DESeq2 (v1.30.1). We used cluster Profiler to perform GO enrichment analysis on the DEGs and calculated  $P \text{ adj} = P_k \text{ value} * n/k$  by hypergeometric distribution method with Benjamini correction (the standard of significant enrichment is  $P \text{ adj} \leq 0.05$ ). Cluster Profiler (v3.18.1) software was used to carry out the enrichment analysis of the KEGG pathway of DEGs, focusing on the significant enrichment pathway with  $P$ -value  $< 0.05$ . Sequencing service was provided by Bioy Biotechnology Co., Ltd. Wuhan, China.

For the quantitative analysis of CIP2A expression in the MDD GEO datasets, we downloaded the original data of the three GEO datasets (GSE54572, GSE54565, and GSE54571), imported the downloaded data into “R” software, converted the gene IDs in the “R” software, and found CIP2A gene and its expression level. The average CIP2A mRNA levels in control group in each GEO dataset were set to “1,” and the data from the three datasets together were normalized by calculating the ratios of (actual CIP2A mRNA level)/(average CIP2A mRNA level in control group) for each sample and were performed Student’s  $t$ -test analysis.

### Statistical analysis

Data were analyzed using GraphPad Prism version 9.0 in a blinded manner. Data were shown as the mean  $\pm$  SEM. For data following normal distribution, differences between groups were evaluated by Student’s  $t$ -test or one-way analysis of variance tests. Two-way repeated-measures ANOVA followed by Bonferroni’s *post hoc* test was used to analyze the difference in Sholl analysis. The method of statistical test for each figure was stated in the figure legend.  $*P < 0.05$ ,  $**P < 0.01$ ,  $***P < 0.001$ ,  $****P < 0.0001$ ,  $P < 0.05$  was considered statistically significant. The  $n$  for each comparison group is stated in each figure legend.

### Data availability

The raw data of RNA-seq in this study were deposited at SRA database with the SRA accession SRP385569 (<https://www.ncbi.nlm.nih.gov/sra/SRP385569>).

**Expanded View** for this article is available [online](#).

### Acknowledgment

This work was supported by the National Natural Science Foundation of China (31970964, 82171426, and 31900685).

### Author contributions

**Rong Liu:** Resources; project administration; writing—review and editing. **Wenting Hu:** Data curation; methodology; writing—original draft. **Zhenyu Liuyang:** Investigation; methodology. **Yuan Tian:** Methodology. **Jiawei Liang:** Methodology. **Xiaolin Zhang:** Methodology. **Huiliang Zhang:** Methodology. **Guan Wang:** Methodology. **Yuda Huo:** Methodology. **Yangping Shentu:** Resources. **Jian-Zhi Wang:** Resources. **Xiaochuan wang:** Resources. **Youming Lu:** Resources. **Jukka Westermarck:** Writing—review and editing. **Hengye Man:** Writing—review and editing.

### Disclosure and competing interests statement

The authors declare that they have no conflict of interest.

### References

- Abe-Higuchi N, Uchida S, Yamagata H, Higuchi F, Hobara T, Hara K, Kobayashi A, Watanabe Y (2016) Hippocampal Sirtuin 1 signaling mediates depression-like behavior. *Biol Psychiatry* 80: 815–826
- Andrabi S, Gjoerup OV, Kean JA, Roberts TM, Schaffhausen B (2007) Protein phosphatase 2A regulates life and death decisions via Akt in a context-dependent manner. *Proc Natl Acad Sci USA* 104: 19011–19016
- Atwal JK, Massie B, Miller FD, Kaplan DR (2000) The TrkB-Shc site signals neuronal survival and local axon growth via MEK and P13-kinase. *Neuron* 27: 265–277
- Brent DA (2016) Antidepressants and suicidality. *Psychiatr Clin North Am* 39: 503–512
- Buffington SA, Di Prisco GV, Auchtung TA, Ajami NJ, Petrosino JF, Costamattioli M (2016) Microbial Reconstitution Reverses Maternal Diet-Induced Social and Synaptic Deficits in Offspring. *Cell* 165: 1762–1775
- Chang LC, Jamain S, Lin CW, Rujescu D, Tseng GC, Sibille E (2014) A conserved BDNF, glutamate- and GABA-enriched gene module related to human depression identified by coexpression meta-analysis and DNA variant genome-wide association studies. *PLoS One* 9: e90980
- Chen KF, Liu CY, Lin YC, Yu HC, Liu TH, Hou DR, Chen PJ, Cheng AL (2010) CIP2A mediates effects of bortezomib on phospho-Akt and apoptosis in hepatocellular carcinoma cells. *Oncogene* 29: 6257–6266
- Conrad CD (2008) Chronic stress-induced hippocampal vulnerability: the glucocorticoid vulnerability hypothesis. *Rev Neurosci* 19: 395–411
- David DJ, Samuels BA, Rainer Q, Wang JW, Marsteller D, Mendez I, Drew M, Craig DA, Guiard BP, Guilloux JP et al (2009) Neurogenesis-dependent and -independent effects of fluoxetine in an animal model of anxiety/depression. *Neuron* 62: 479–493
- Dowlati Y, Herrmann N, Swardfager WL, Reim EK, Lanctôt KL (2010) Efficacy and tolerability of antidepressants for treatment of depression in coronary artery disease: a meta-analysis. *Can J Psychiatry* 55: 91–99
- Duman RS (2013) Remodeling chromatin and synapses in depression. *Nat Med* 19: 267–268
- Duman RS, Aghajanian GK (2012) Synaptic dysfunction in depression: potential therapeutic targets. *Science* 338: 68–72
- Ehm O, Göritz C, Covic M, Schäffner I, Schwarz TJ, Karaca E, Kempkes B, Kremmer E, Pfrieger FW, Espinosa L et al (2010) RBPJkappa-dependent signaling is essential for long-term maintenance of neural stem cells in the adult hippocampus. *J Neurosci* 30: 13794–13807
- Fava M (2003) Diagnosis and definition of treatment-resistant depression. *Biol Psychiatry* 53: 649–659

- Gao H, Li Y, Lin T, Cheng Y, Ma Y (2020) Downregulation of CIP2A inhibits cancer cell proliferation and vascularization in renal clear cell carcinoma. *Biomed Pap Med Fac Univ Palacky Olomouc Czech Repub* 164: 196–202
- He JG, Zhou HY, Xue SG, Lu JJ, Xu JF, Zhou B, Hu ZL, Wu PF, Long LH, Ni L et al (2021) Transcription factor TWIST1 integrates dendritic remodeling and chronic stress to promote depressive-like behaviors. *Biol Psychiatry* 89: 615–626
- Hill MN, Hellems KG, Verma P, Gorzalka BB, Weinberg J (2012) Neurobiology of chronic mild stress: parallels to major depression. *Neurosci Biobehav Rev* 36: 2085–2117
- Holtzheimer PE, Mayberg HS (2011) Stuck in a rut: rethinking depression and its treatment. *Trends Neurosci* 34: 1–9
- Howard DM, Adams MJ, Clarke TK, Hafferty JD, Gibson J, Shirali M, Coleman JRI, Hagenaars SP, Ward J, Wigmore EM et al (2019) Genome-wide meta-analysis of depression identifies 102 independent variants and highlights the importance of the prefrontal brain regions. *Nat Neurosci* 22: 343–352
- Jaworski J, Spangler S, Seeburg DP, Hoogenraad CC, Sheng M (2005) Control of dendritic arborization by the phosphoinositide-3'-kinase-Akt-mammalian target of rapamycin pathway. *J Neurosci* 25: 11300–11312
- Jiang W, Tang YY, Zhu WW, Li C, Zhang P, Li RQ, Chen YJ, Zou W, Tang XQ (2021) PI3K/AKT pathway mediates the antidepressant- and anxiolytic-like roles of hydrogen sulfide in streptozotocin-induced diabetic rats via promoting hippocampal neurogenesis. *Neurotoxicology* 85: 201–208
- Junttila MR, Puustinen P, Niemelä M, Ahola R, Arnold H, Böttzauw T, Ala-aho R, Nielsen C, Ivaska J, Taya Y et al (2007) CIP2A inhibits PP2A in human malignancies. *Cell* 130: 51–62
- Kempton MJ, Salvador Z, Munafò MR, Geddes JR, Simmons A, Frangou S, Williams SC (2011) Structural neuroimaging studies in major depressive disorder. Meta-analysis and comparison with bipolar disorder. *Arch Gen Psychiatry* 68: 675–690
- Kerosuo L, Fox H, Perälä N, Ahlqvist K, Suomalainen A, Westermarck J, Sariola H, Wartiovaara K (2010) CIP2A increases self-renewal and is linked to Myc in neural progenitor cells. *Differentiation* 80: 68–77
- Kolb B, Wishaw IQ (1998) Brain plasticity and behavior. *Annu Rev Psychol* 49: 43–64
- Krishnan V, Han MH, Mazei-Robison M, Iñiguez SD, Ables JL, Vialou V, Berton O, Ghose S, Covington HE 3rd, Wiley MD et al (2008) AKT signaling within the ventral tegmental area regulates cellular and behavioral responses to stressful stimuli. *Biol Psychiatry* 64: 691–700
- Kumar V, Zhang MX, Swank MW, Kunz J, Wu GY (2005) Regulation of dendritic morphogenesis by Ras-PI3K-Akt-mTOR and Ras-MAPK signaling pathways. *J Neurosci* 25: 11288–11299
- Ledford H (2014) Medical research: if depression were cancer. *Nature* 515: 182–184
- Li N, Lee B, Liu RJ, Banas M, Dwyer JM, Iwata M, Li XY, Aghajanian G, Duman RS (2010) mTOR-dependent synapse formation underlies the rapid antidepressant effects of NMDA antagonists. *Science* 329: 959–964
- Li N, Liu RJ, Dwyer JM, Banas M, Lee B, Son H, Li XY, Aghajanian G, Duman RS (2011) Glutamate N-methyl-D-aspartate receptor antagonists rapidly reverse behavioral and synaptic deficits caused by chronic stress exposure. *Biol Psychiatry* 69: 754–761
- Li W, Liu X, Qiao H (2020) Downregulation of hippocampal SIRT6 activates AKT/CRMP2 signaling and ameliorates chronic stress-induced depression-like behavior in mice. *Acta Pharmacol Sin* 41: 1557–1567
- Liang S, Wang Q, Kong X, Deng W, Yang X, Li X, Zhang Z, Zhang J, Zhang C, Li XM et al (2019) White matter abnormalities in major depression biotypes identified by diffusion tensor imaging. *Neurosci Bull* 35: 867–876
- Malhi GS, Mann JJ (2018) Depression. *Lancet* 392: 2299–2312
- Markus A, Patel TD, Snider WD (2002) Neurotrophic factors and axonal growth. *Curr Opin Neurobiol* 12: 523–531
- McIntyre RS, Filteau MJ, Martin L, Patry S, Carvalho A, Cha DS, Barakat M, Miguelez M (2014) Treatment-resistant depression: definitions, review of the evidence, and algorithmic approach. *J Affect Disord* 156: 1–7
- Nestler EJ, Barrot M, DiLeone RJ, Eisch AJ, Gold SJ, Monteggia LM (2002) Neurobiology of depression. *Neuron* 34: 13–25
- Peineau S, Taghibiglou C, Bradley C, Wong TP, Liu L, Lu J, Lo E, Wu D, Saule E, Bouschet T et al (2007) LTP inhibits LTD in the hippocampus via regulation of GSK3beta. *Neuron* 53: 703–717
- Price JL, Drevets WC (2010) Neurocircuitry of mood disorders. *Neuropsychopharmacology* 35: 192–216
- Puustinen P, Jäättelä M (2014) KIAA1524/CIP2A promotes cancer growth by coordinating the activities of MTORC1 and MYC. *Autophagy* 10: 1352–1354
- Qiao H, An SC, Ren W, Ma XM (2014) Progressive alterations of hippocampal CA3-CA1 synapses in an animal model of depression. *Behav Brain Res* 275: 191–200
- Read DE, Gorman AM (2009) Involvement of Akt in neurite outgrowth. *Cell Mol Life Sci* 66: 2975–2984
- Rosso SB, Sussman D, Wynshaw-Boris A, Salinas PC (2005) Wnt signaling through Dishevelled, Rac and JNK regulates dendritic development. *Nat Neurosci* 8: 34–42
- Sedmak D, Hrvoj-Mihic B, Džaja D, Habek N, Uylings HB, Petanjek Z (2018) Biphasic dendritic growth of dorsolateral prefrontal cortex associative neurons and early cognitive development. *Croat Med J* 59: 189–202
- Shentu YP, Hu WT, Zhang Q, Huo Y, Liang JW, Liuyang ZY, Zhou H, Wei H, Ke D, Wang XC et al (2019) CIP2A-promoted astrogliosis induces AD-like synaptic degeneration and cognitive deficits. *Neurobiol Aging* 75: 198–208
- Shentu YP, Huo Y, Feng XL, Gilbert J, Zhang Q, Liuyang ZY, Wang XL, Wang G, Zhou H, Wang XC et al (2018) CIP2A causes tau/APP phosphorylation, synaptopathy, and memory deficits in Alzheimer's disease. *Cell Rep* 24: 713–723
- Sibille E (2014a) Gene Expression Omnibus GSE54572 (<https://www.ncbi.nlm.nih.gov/geo/query/acc.cgi?acc=GSE54572>). [DATASET]
- Sibille E (2014b) Gene Expression Omnibus GSE54565 (<https://www.ncbi.nlm.nih.gov/geo/query/acc.cgi?acc=GSE54565>). [DATASET]
- Sibille E (2014c) Gene Expression Omnibus GSE54571 (<https://www.ncbi.nlm.nih.gov/geo/query/acc.cgi?acc=GSE54571>). [DATASET]
- Sjöberg L, Karlsson B, Atti AR, Skoog I, Fratiglioni L, Wang HX (2017) Prevalence of depression: comparisons of different depression definitions in population-based samples of older adults. *J Affect Disord* 221: 123–131
- Tavosanis G (2012) Dendritic structural plasticity. *Dev Neurobiol* 72: 73–86
- Vanderplow AM, Eagle AL, Kermath BA, Bjornson KJ, Robison AJ, Cahill ME (2021) Akt-mTOR hypoactivity in bipolar disorder gives rise to cognitive impairments associated with altered neuronal structure and function. *Neuron* 109: 1479–1496.e1476
- Vauzour D, Corsini S, Müller M, Spencer JPE (2018) Inhibition of PP2A by hesperetin may contribute to Akt and ERK1/2 activation status in cortical neurons. *Arch Biochem Biophys* 650: 14–21
- Ventelä S, Côme C, Mäkelä JA, Hobbs RM, Mannermaa L, Kallajoki M, Chan EK, Pandolfi PP, Toppari J, Westermarck J (2012) CIP2A promotes proliferation of spermatogonial progenitor cells and spermatogenesis in mice. *PLoS One* 7: e33209
- Wang M, Yang L, Chen Z, Dai L, Xi C, Wu X, Wu G, Wang Y, Hu J (2021) Geniposide ameliorates chronic unpredictable mild stress induced depression-like behavior through inhibition of ceramide-PP2A signaling via the PI3K/Akt/GSK3β axis. *Psychopharmacology (Berl)* 238: 2789–2800

- Willner P (2005) Chronic mild stress (CMS) revisited: consistency and behavioural-neurobiological concordance in the effects of CMS. *Neuropsychobiology* 52: 90–110
- Willner P, Towell A, Sampson D, Sophokleous S, Muscat R (1987) Reduction of sucrose preference by chronic unpredictable mild stress, and its restoration by a tricyclic antidepressant. *Psychopharmacology (Berl)* 93: 358–364
- Wray NR, Ripke S, Mattheisen M, Trzaskowski M, Byrne EM, Abdellaoui A, Adams MJ, Agerbo E, Air TM, Andlauer TMF et al (2018) Genome-wide association analyses identify 44 risk variants and refine the genetic architecture of major depression. *Nat Genet* 50: 668–681
- Xu WS, Sun X, Song CG, Mu XP, Ma WP, Zhang XH, Zhao CS (2016) Bumetanide promotes neural precursor cell regeneration and dendritic development in the hippocampal dentate gyrus in the chronic stage of cerebral ischemia. *Neural Regen Res* 11: 745–751
- Yu X, Malenka RC (2003) Beta-catenin is critical for dendritic morphogenesis. *Nat Neurosci* 6: 1169–1177